25th ABCM International Congress of Mechanical Engineering
October 20-25, 2019, Uberlândia, MG, Brazil

COB-2019-1007
NUMERICAL ANALYSIS OF AN UNGLAZED SOLAR POOL COLLECTOR

Felipe Venancio Mitkiewicz Silva
Antônia Sônia Alves Cardoso Diniz
Daniel Sena Braga
Lucas Paglioni Pataro Faria
Elvis Mayk Chaves Barbosa
Vinicius Augusto Camatta Santana
Cristiana Brasil Maia
Pontifícia Universidade Católica de Minas Gerais, Av. Dom José Gaspar, 500 Coração Eucarístico - Belo Horizonte MG 30535-901
felipemit@hotmail.com, asacd@pucminas.br, danielsb@pucminas.br, lucas.faria@pucminas.br, elvismayk@pucminas.br, viniciusbh@msn.com, cristiana@pucminas.br

Abstract. *Solar pool heating systems are used to convert the sun's electromagnetic radiation into heat to warm swimming pool's water. Those systems are generally composed of a solar collector, a filter, a pump, and a flow control valve. In order to guarantee the quality, the unglazed solar pool collectors are tested by regulations and then ranked based on their thermal efficiency. The ABNT NBR 15747 standards regulate about those tests in Brazil. A real solar pool collector has been tested under those standards at the Pontifical Catholic University of Minas Gerais Solar Laboratory. The test and its results were the basis of this paper, which proposes a numerical analysis of the tested unglazed solar pool collector. The numerical analysis used computational fluid dynamics, based on finite volumes method, to simulate the same conditions. Therefore, the numerical results were validated by comparing with the experimental data. The numerical parameter used to validate was the outlet mean temperature, which differed only 0.1 °C from the experimental data.*

Keywords: *Unglazed solar collector, numerical analysis, solar thermal energy, cfd.*

1. INTRODUCTION

The attention of the world has been addressed to climate change after authorities have stressed the threat relevance from the effects of global greenhouse gas emissions for the humankind, at COP 21 (United Nations, 2015). Seeking to reduce the effects of the climate change, the parties consented on Paris Agreement, among other terms, to promote universal access to sustainable energy in developing countries. Under those circumstances, solar energy is considered a valid alternative to accomplish those goals, not only because it is a renewable source of energy but also because of its versatility. For example, it can provide electricity through photovoltaic cells and thermal energy through solar collectors.

There are different types of solar thermal applications contributing to reduce the CO_2 emissions, for example, space heating, heating of industrial processes, solar district heating and swimming pool heating. This last one usually is composed of a solar collector, a filter, a pump and a flow control valve. The swimming pool solar heater system uses unglazed collectors to convert electromagnetic radiation from the sun into heat to warm pool's water due to its simplicity and cost-benefit.

Unglazed water collector represents 6 % of the total solar collectors installed worldwide and 4 % of energy saving of glazed and unglazed solar collector in operations in 2014. It represented a final energy saving of 1.4 million tons of oil and 4.6 million tons of CO_2 (IEA, 2016).

In order to accomplish with regulations and then be able to be on the market, the thermal efficiency of the solar collector must be assured by the manufacturers. Numerical simulations can be used to reduce the validation process time. Corgozinho (2015) applied the finite volume method in the evaluation of a flat plate solar collector performance, based on a three-dimensional model of a collector with seven risers and double glass cover, and had satisfactory results. Indeed, the vast majority of the papers found in the literature concentrate on flat plate collectors, for bath purposes. For example, Pandey and Chaurasiya (2017) did a review on the analysis and development of solar flat plate collector and Tagliafico et al. (2014) presented a review of dynamic thermal models and CFD analysis for flat-plate thermal solar collectors. In fact, there were not many papers regarding solar pool collectors. On the other hand, the flat plate collectors main studies focus mostly in the improvement on the thermal efficiency of those collectors (Missirlis et al., 2014)(Ángel, Manuel et al., 2013), frequently is used computational fluid dynamics (CFD) techniques (Gunjo et al. , 2017)(Martinopoulos et al.,

2010), mainly when the experimental analysis is not feasible. The same line of study can be applied for solar pool collector and this paper aims to contribute for this scarce field of study

The unglazed pool collectors are used to heat the water and keep the thermal comfort of the swimming pools. In order to guarantee the quality, those collectors are regulated by standards, which in Brazil is the ABNT NBR 15747. A real polymeric solar pool collector was tested under those standards at the Solar Laboratory located in Pontifical Catholic University of Minas Gerais (GREEN PUC Minas). The test conditions and its results were the basis of the present work, the numerical analysis of the fluid dynamics on a virtual unglazed solar pool collector. Moreover, the numerical analysis was performed through CFD, using Ansys' Fluent Solver. Rangababu et al., (2015) used Fluent to verify heat transfer mechanism of flat plate collectors and obtained success in validating the model with the experimental data. Finally, this paper used the analysis to ascertain the accuracy of a simulation by comparing the fluid temperature in the upper manifold outlet, also known as the header pipe.

2. MATHEMATICAL MODELLING

The governing differential equations are used for the analysis and description of the fluid motion. They are Conservation of Mass Eq. (1), Momentum Eq. (2), and Energy Eq. (3), as described below (Batchelor, 1967):

$$\frac{\partial \rho}{\partial t} + \nabla.(\rho.\vec{v}) = 0 \tag{1}$$

$$\frac{\partial}{\partial t}(\rho.\vec{v}) + \nabla.(\rho.\vec{v}.\vec{v}) = -\nabla \mathrm{p} + \nabla.\left(\mu\left[(\nabla\vec{v} + \nabla\vec{v}^{T}) - \frac{2}{3}\nabla.\vec{v}I\right]\right) + \rho\vec{g} \tag{2}$$

$$\frac{\partial}{\partial t}(\rho E) + \nabla.\left(\vec{v}(\rho E + p)\right) = \nabla.\left(k_{eff}\nabla \mathrm{T} - \mathrm{h}\vec{\mathrm{J}} + \left(\mu\left[(\nabla\vec{v} + \nabla\vec{v}^{T}) - \frac{2}{3}\nabla.\vec{v}I\right].\vec{v}\right)\right) \tag{3}$$

Transient and random fluctuations of the flow properties generate a turbulent pattern, consequently, the analytical approach is unusable in this problem. In addition, it is a three-dimensional flow and the Reynolds number at the inlet pipe was higher than 2300. In order to consider the turbulence effects on simulation, this work used the realizable k – ε turbulence model (Shih, Liou, Shabbir, Yang, and Zhu, 1995). This model differs from the standard k – ε (Launder and Spalding, 1972) (Versteeg; Malalasekera, 1995) due to a new model equation for dissipation, ε , based on the dynamic equation of the mean-square velocity fluctuation and a new eddy viscosity formula involving a variable C_μ originally proposed by Reynolds (1987). The realizable k – ε model uses the concept of turbulent(eddy) viscosity and has transport equations for turbulent kinetic energy (k), Eq. (4), and its rate of dissipation (ε), Eq. (5). The realizable k – ε equations are:

$$\frac{\partial}{\partial t}(\rho k) + \frac{\partial}{\partial x_j}(\rho k u_j) = \frac{\partial}{\partial x_j}\left[\left(\mu + \frac{\mu_t}{\sigma_k}\right)\frac{\partial k}{\partial x_j}\right] + G_k + G_b - \rho\varepsilon - Y_M + S_k \tag{4}$$

$$\frac{\partial}{\partial t}(\rho \varepsilon) + \frac{\partial}{\partial x_j}(\rho \varepsilon u_j) = \frac{\partial}{\partial x_j}\left[\left(\mu + \frac{\mu_t}{\sigma_\varepsilon}\right)\frac{\partial \varepsilon}{\partial x_j}\right] + \rho C_1 S\varepsilon - \rho C_2 \frac{\varepsilon^2}{k + \sqrt{\nu\varepsilon}} + C_{1\varepsilon}\frac{\varepsilon}{k}C_{3\varepsilon}G_b + S_\varepsilon \tag{5}$$

where

$$C_1 = \max\left[0.43, \frac{\eta}{\eta + 5}\right], \qquad \eta = \mathrm{S}\frac{k}{\varepsilon}, \qquad \mathrm{S} = \sqrt{2S_{ij}S_{ij}} \tag{6}$$

Where ρ is the fluid density (kg/m^3), t is time (s), k is turbulent kinetic energy (J/kg), ε is turbulent kinetic energy rate of dissipation (J/kg.s), *x* is the cartesian coordinate variable (m), μ is dynamic viscosity (Pa.s) , μ_t is the turbulent viscosity (Pa.s), *u* is velocity magnitude on *x* direction (m/s), σ_k and σ_ε are the turbulent Prandtl numbers for k and ε respectively. G_k is the turbulent kinetic energy due to mean velocity gradients (J/kg), G_b is the turbulent kinetic energy due to buoyancy (J/kg) and Y_M the contribution of the fluctuating dilatation in compressible turbulence to the overall dissipation rate (J/kg). The values of $C_{1\varepsilon}$, C_2 and $C_{3\varepsilon}$ are constants, while S_k and S_ε terms are set by the user. Finally, μ_t is defined as:

$$\mu_t = \rho \mathrm{C}_\mu \frac{k^2}{\varepsilon} \tag{7}$$

Notably, C_μ is no longer a constant as it is in standard k-ε, it is computed as:

$$C_\mu = \frac{1}{A_0 + A_S \frac{kU^*}{\varepsilon}} \tag{8}$$

where

$$U^* = \sqrt{S_{ij}S_{ij} + \widetilde{\Omega}_{ij}\widetilde{\Omega}_{ij}}, \qquad \widetilde{\Omega}_{ij} = \Omega_{ij} - 2\varepsilon_{ijk}\omega_k, \qquad \Omega_{ij} = \overline{\Omega_{ij}} - \varepsilon_{ijk}\omega_k \tag{9}$$

S_{ij} is the mean rate of strain tensor (s^{-1}), Ω_{ij} is the mean rate of rotation tensor (s^{-1}) and $\overline{\Omega_{ij}}$ is the mean rate of tensor viewed in a moving reference with the angular velocity ω_k (rad/s). In addition, the model constants are given by:

$$A_0 = 4.04, \qquad A_S = \sqrt{6}cos\varphi \tag{10}$$

and

$$\varphi = \frac{1}{3}\cos^{-1}\left(\sqrt{6}W\right), \qquad W = \frac{S_{ij}S_{jk}S_{ki}}{\tilde{S}^3}, \qquad \tilde{S} = \sqrt{S_{ij}S_{ij}}, \qquad S_{ij} = \frac{1}{2}\left(\frac{\partial u_j}{\partial x_i} + \frac{\partial u_i}{\partial x_j}\right) \tag{11}$$

The model constants $C_{1\varepsilon}$, C_2, σ_k, and σ_ε have been established to ensure that the model performs well for certain canonical flows. They are:

$$C_{1\varepsilon} = 1.44, \qquad C_2 = 1.9, \qquad \sigma_k = 1.0, \qquad \sigma_\varepsilon = 1.2 \tag{12}$$

3. METHODOLOGY

The unglazed solar pool collector is used to provide thermal comfort on swimming pools. Thus, in order to guarantee the quality, Brazilian regulation ranks the solar collectors based on their specific monthly energy production, which is directly proportional to their mean thermal efficiency (INMETRO, 2012). The ABNT NBR 15747 standards specify the test methods for the validation of the durability, reliability, safety and thermal performance requirements of solar fluid heating collectors, including testing methods for the characterization of the thermal performance of liquid heating collectors. Thus, the thermal performance was tested on a 2x1 unglazed solar collector, through the ABNT NBR 15747 standards, in a solar simulator accredited laboratory at GREEN PUC Minas. The solar simulator is presented in Figure 1.

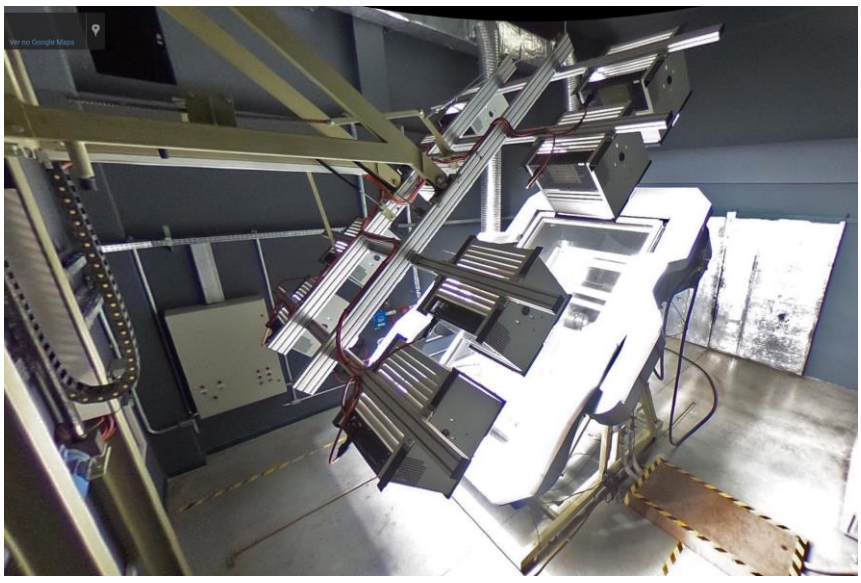

Figure 1 - Solar Simulator Laboratory in PUC Minas
Available in: http://ipuc.pucminas.br/green/galeria.html

After the trial has been completed, a numerical analysis was developed in other to simulate one of the trial steps. A virtual solid of the solar collector was created and then simulated through CFD and finite volume method (FVM) on the same conditions of the real domain. The results were compared to the experimental data to validate the numerical analysis.

3.1 Real Domain

The real domain is defined as a real unglazed solar pool collector made by polypropylene with 85 lead pipes. Table 1 presents the collector geometric details.

Table 1 - Unglazed pool collector geometric characteristics.

	Lead Pipes (m)	Manifolds (m)
Internal Diameter	0.0065	0.0270
External Diameter	0.0085	0.0320
Length	1.9350	1.0100

The gross external area is 1.88 m^2, the dry collector weight is 4.70 kg while filled up with water is 11.12 kg. Finally, its working pressure is determined as 55.15 kPa.

The trial steps were based on ABNT NBR 15747 procedures and it requests that the collector had to be tilted in 45° (*xy* plane). Moreover, the heat flux was set as constant radiation of 815 W/m^2 and the mass flow rate was adjusted to be around 0.13 kg/s, by a pump, at the entrance of the lower manifold, on *z* direction. Additionally, parallel to the absorber area, it was set up a wind flow at speed of 1.5 m/s ± 0.5 m/s, as regulated by Brazilian National Institute of Metrology, Quality and Technology (INMETRO, 2012). Figure 2 shows the solid orientation, as well as the fluid path on it (the fluid enters in the lower manifold inlet, goes up through lead pipes, receives the heat from the wall, ending up to the upper manifold outlet). It was verified it was a turbulent flow, as the Reynolds Number was higher than 2300, precisely, 6905. Finally, data as, inlet, outlet, and environment temperatures, also fluid density and specific heat ratio, among others, were acquired in order to verify the thermal efficiency of the solar collector and its specific monthly energy production. Table 2 presents the experimental results.

Table 2 - Experimental Results

Trial Step	Solar Radiation (W/m^2)	Mass Flow Rate (kg/s)	Temperature (°C)			
			Environment	Inlet	Outlet	ΔT
1	815	0.13	23.8	24.0	26.1	2.1
2	815	0.13	24.6	26.3	28.2	1.9
3	815	0.13	25.6	28.8	30.6	1.7
4	815	0.13	27.1	32.7	34.1	1.4
5	815	0.13	26.6	30.1	31.8	1.7
6	815	0.13	26.8	28.4	30.4	1.9
7	815	0.13	26.7	26.5	28.7	2.2

3.2 Virtual Domain

The virtual domain is the real model discretized as a virtual unglazed solar pool collector. The 3D model was developed on Solidworks®, based on the real model, and sequentially, a mesh was created on Ansys®. In the end, the mesh has 2.88E+07 elements and 6.46E+06 nodes. The mesh size was directly linked with the slenderness of the geometry, as the lead pipes had an inner diameter of 6.5 mm and length of almost 2000.0 mm and the manifolds had an inner diameter of 27.0 mm and approximately 1000.0 mm length, as can be seen in Table 1. Figure 2 presents the solar collector details. In addition, in this paper, due to the size of the mesh, it was only validated the 7^{th} trial step, in other to reduce the time demanded to solve the problem on Ansys®.

Thus, it was used the Fluent solver from Ansys® to run the simulation and was selected the energy and turbulence realizable k-ε models (turbulent flow at the inlet manifold) to define the physics in which the solar collector was tested. Another relevant point is that the fluid flow was characterized as a steady state condition.

Moreover, some assumptions were made before running the simulation. Firstly, (1) it was assumed a uniform wall heat flux on the absorber surface, oriented normal to the incidence of the direct normal radiation (Bejan, 2013). However, in order to consider optical thermal losses, the constant heat flux was defined as 733.5 W/m^2, which is 0.90 of the experimental value (Streicher, 2016). On the other hand, (2) the back of the absorber surface was considered adiabatic. Additionally, (3) fluid density was considered to be constant and (4) the solar collector body was neglected on the simulation. Also, (5) gravity was defined as 9.81 m/s^2.

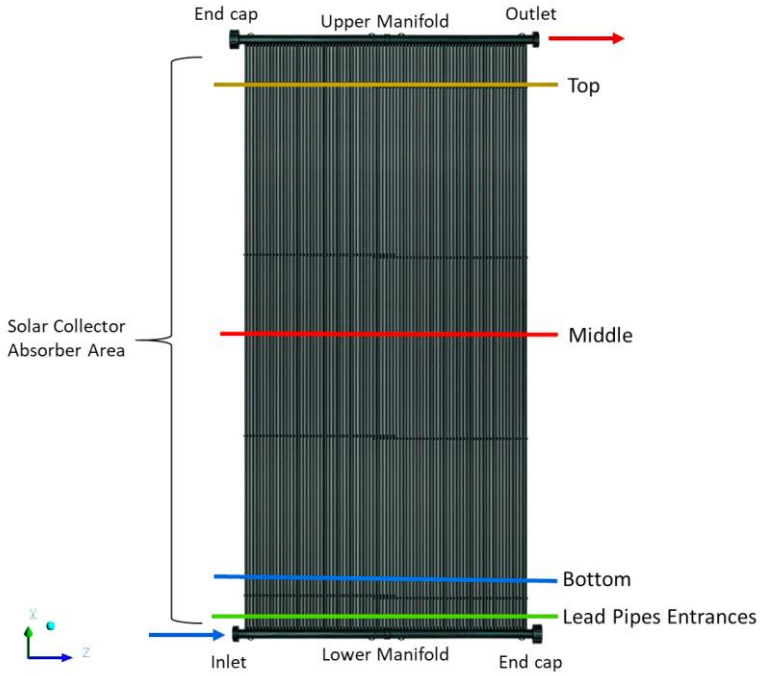

Figure 2 – Solar Collector details.

The simulation results were acquired from the manifolds and different locations on the lead pipes, (from the bottom, middle and top) as Figure 2 shows.

4. RESULTS AND DISCUSSION

The unglazed solar pool collector thermal efficiency reported by GREEN PUC Minas laboratory was 41.84 % and the calculations were based on Portaria 301 (INMETRO, 2012). The numerical results are displayed from Figure 3 up to Figure 9. Figure 3 shows the mean temperature distribution along the upper surface of the solar collector, in other words, the absorber plate.

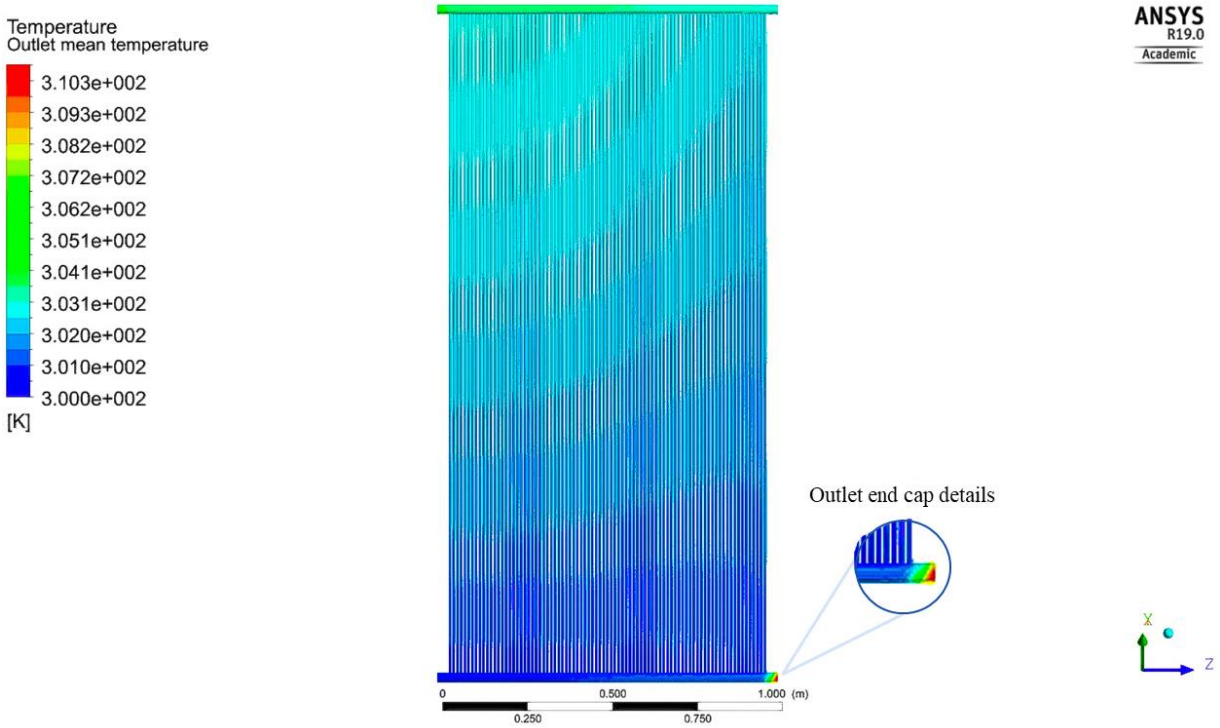

Figure 3 – Mean temperatures on solar collector

As can be seen at the 7th trial step, the inlet temperature was 299.6 K (26.5 °C), while the environment was 299.9 K (26.7 °C). Notably, Figure 3 presents the highest temperature of 310.3 K (37.1 °C) at the edge of the lower manifold in the end cap, in contrast, the lowest temperature was located at the entrance of the inlet lower manifold, the other extremity. Figure 3 also displays that the absorber solar collector area didn't show a linear mean temperature distribution pattern, it shows that upper left side of the surface has shown to have higher temperatures when compared with the lower right side of the area. In the same fashion, velocity vectors distribution has shown to have a similar pattern as the mean temperature distribution, as presented in Figure 4.

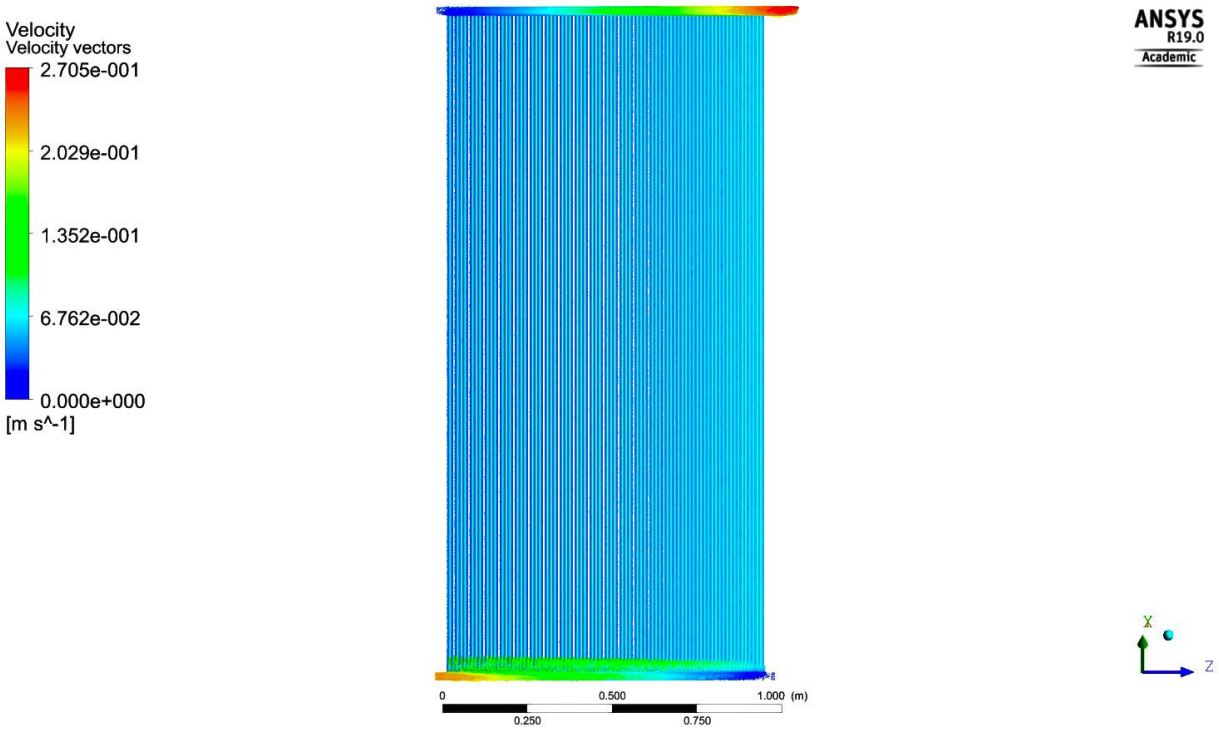

Figure 4 – Velocity vectors on solar collector.

The highest velocity vectors occur at the end of the upper manifold, on the outlet, reaching almost 0.28 m/s. On the other hand, the lowest velocity vectors appeared in both end caps with magnitudes of almost 0 m/s. Figure 5 shows the velocity vectors details on the lower manifold. In fact, as the end caps are enclosed, there is no way to water flow, consequently, there are very few velocity vectors.

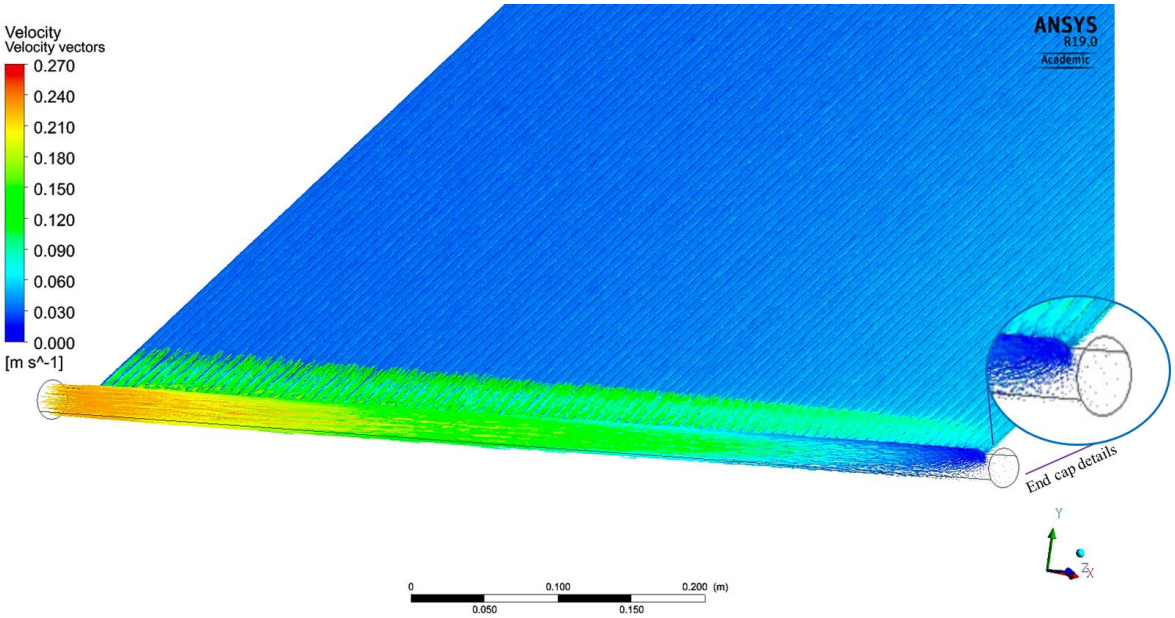

Figure 5 - Fluid velocity details on the bottom of the solar collector.

Indeed, the reduced magnitude of fluid motion increases water temperature on those locations, as Figure 3 presents. The highest temperature, as mentioned before, occurs at the end caps, mainly on the end cap on the lower manifold, highlighted in red color. In addition, as the inlet flow on the lower manifold is turbulent, at the beginning of the lead pipes, the velocity vectors were slightly faster than the following velocity vectors of the fluid in flow direction, as can be seen by the green color on Figure 5. Figure 6 shows the fluid velocity along the *z* and *y* directions, from left to right on *z*, and at the top, middle, bottom, and lead pipe entrances, on *y*.

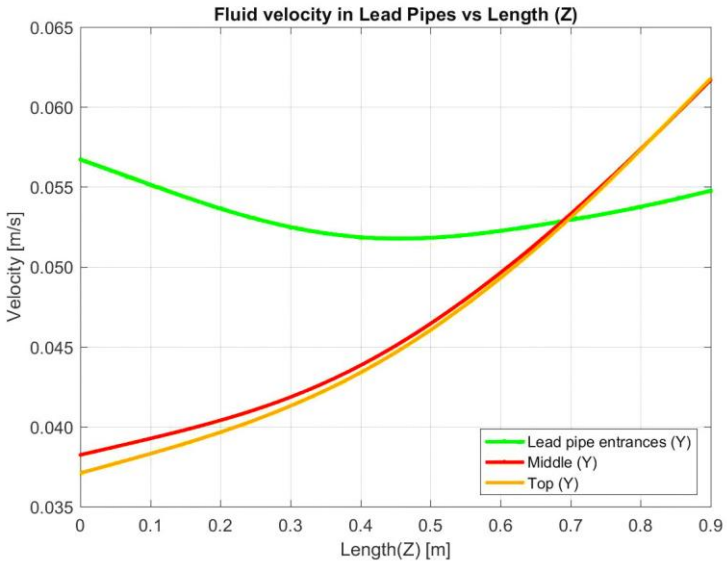

Figure 6 - Fluid velocity vs position (*y* and *z*)

As mentioned before, notably, the fluid velocity is higher at the lead pipe entrances, however, it is overtaken by the magnitudes of all fluid velocities, in the right side, approximately at 0.7 m in z. Figure 6 pointed out that the fluid velocity of the middle and the top increase in a nonlinear fashion along *z* direction. Additionally, neglecting the lead pipe entrances, the top and the middle velocity curves have similar behaviors.

Figure 5 and Figure 6 also show that the manifold doesn't provide uniform flow to the lead pipes, unlike Duffie and Beckman (2001) have stated that, for flat glazed solar collectors, which construction is of sheet and parallel tube type, the headers would provide uniform flow. This analysis can be done by the fluid velocity curves since the area doesn't change along the lead pipes length in y direction and density was considered constant.

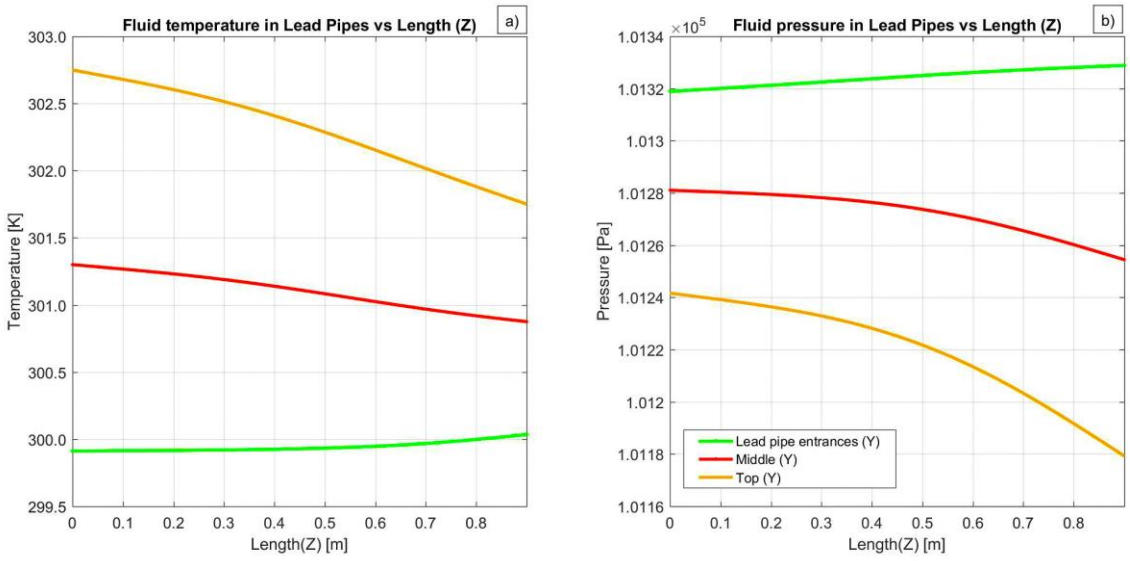

Figure 7 - Lead Pipes a) Temperature along *z* and b) Pressure along *z*

Figure 7 corroborates with the velocity pattern observed in Figure 6, as the right side of collector, has shown to have higher velocities compared with the left side, clearly Figure 7 b) shows that at the right side of the collector occurs the larger difference of pressure, resulting in more pressure energy to promote fluid motion. The same logical reasoning could be applied to Figure 7 a), as can be seen, a higher difference of temperature at the left side of the collector when compared with the right side. This is caused due to the fluid velocity, since the higher is the velocity, the higher is the heat rate and lower the temperature difference, because heat energy is being transported through the fluid towards outside the collector.

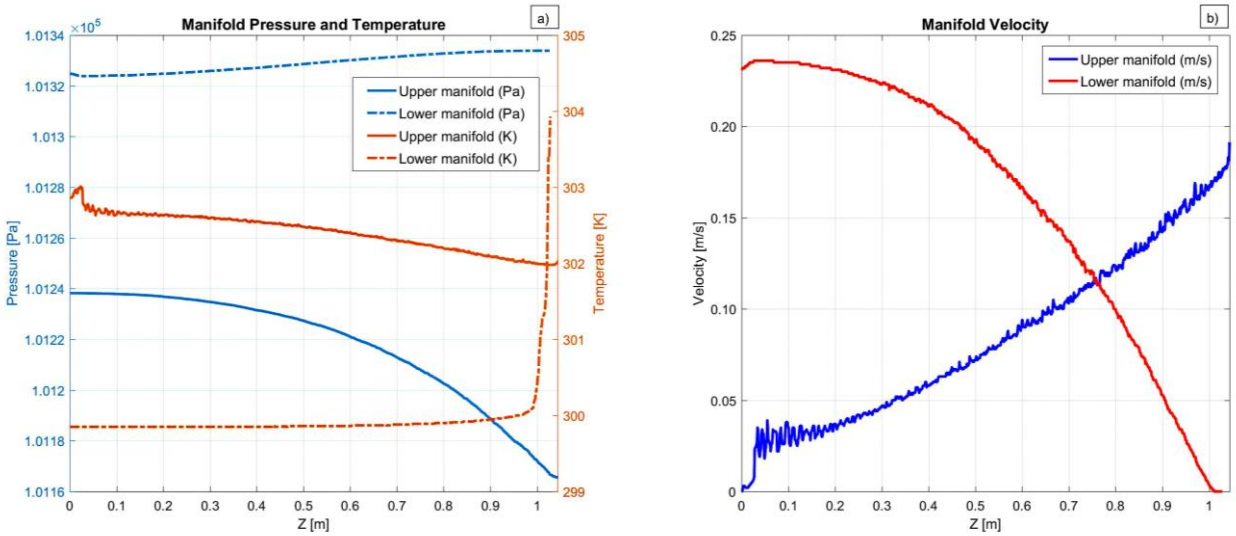

Figure 8 - Manifold a) Pressure and Temperature along *z* and b) Velocity along *z*

Figure 8 a) reinforced Figure 7 b) idea regarding the difference of fluid pressure along z, highlighting the right side of the collector. Important to realize that the higher temperature also occurs at the lower manifold, at the end cap, validating what Figure 3 displayed. Moreover, Figure 8 b) shows that at the end cap on the lower manifold, the fluid reaches 0 m/s, confirming what Figure 5 presented, there are fewer velocity vector at the end cap, suggesting that there is few or almost none fluid motion on that region.

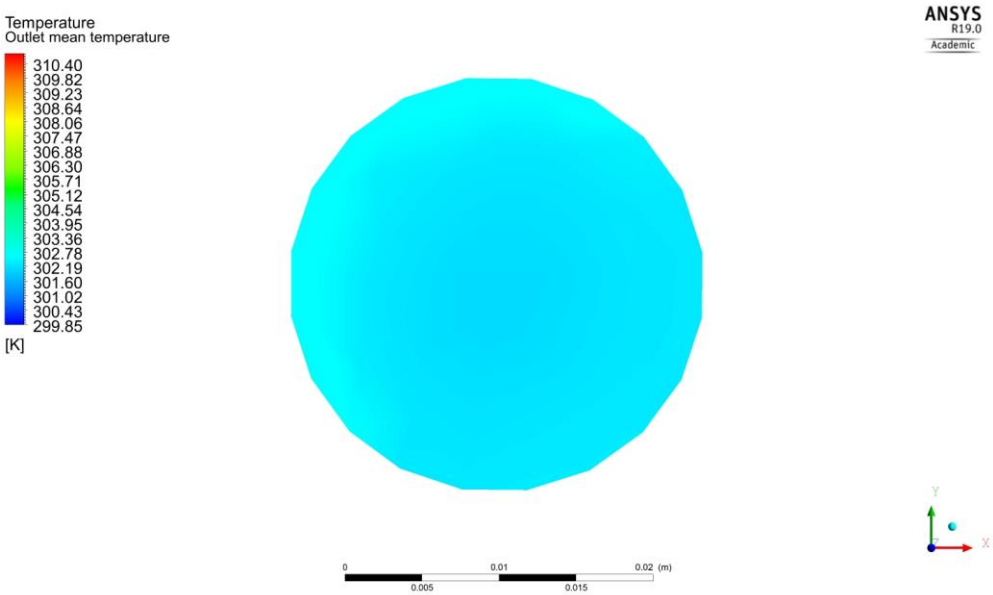

Figure 9 - Upper manifold outlet mean temperature

Finally, Figure 9 shows that the upper manifold outlet mean temperature was 302.0 kelvin (28.8 °C), which is 0.1°C higher than the experimental temperature, which was 28.7 °C, as presented in Table 2 in trial step number 7. This temperature difference validates the numerical analysis since 0.1°C represents only 0.34 % of error.

5. CONCLUSIONS

A numerical simulation of an unglazed solar pool collector was performed through CFD, based on thermal performance tested on a 2x1 unglazed solar collector, through the ABNT NBR 15747 standards, in a solar simulator. The numerical mean outlet temperature on the upper manifold merged with the experimental, then, simulation was validated in the 7th trial step. Furthermore, the simulation is ready to run on the other steps. After the validation, a results analysis was performed, and as can be seen, results pointed out that the right side of the collector has higher velocity vectors and lower temperatures as well, and the opposite occurs on the left side.

There are two hypotheses for the velocity curves behavior presented in Figure 6. It can be a result of how the water fills up the lower manifold, transiently confining an amount of the mass flow rate at the end cap on the lower manifold, resulting in the greatest pressure difference along the *y* direction, then, promoting the fluid motion to be faster on this side of the collector. Nevertheless, this pressure rise can be related to the temperature rising due to the confinement, or it can be the sum of both hypotheses previously discussed.

The solid characteristics, size and its slenderness, resulted in a large number of elements and nodes of the mesh, resulting in required a lot of time processing. In order to attenuate this situation, some assumptions and simplifications were done, and after the results, they are shown to be coherent, as the experimental-numerical temperature difference was considerably short. Another simulation, neglecting some of the simplifications, could provide more data to improve the accuracy of this analysis.

Future works should be taking into account the fluid density variance to verify how it affects the simulation results, also new methods to reduce the complexity and time processing of the problem could be proposed. Finally, new simulations with the other trial steps have to be done to validate the whole spectrum of the trial. Finally, as there are few papers about the unglazed solar pool collectors, this paper is a contribution for this field of research.

6. ACKNOWLEDGEMENTS

The authors are thankful to CNPq, CAPES, FAPEMIG and PUC Minas.

7. REFERENCES

Ángel, M.-D. J., Manuel, O.-R. J., Omar, J.-S., Antonio, Z.-A. M., & Armando, E.-O., 2013. Analysis of Flow and Heat Transfer in a Flat Solar Collector with Rectangular and Cylindrical Geometry Using CFD. *Ingeniería, Investigación y Tecnología*, *14*(4), 553–561.

Batchelor, F. R. S. G. K., 1967. *An Introduction to Fluid Dynamics*. (C. U. Press, Ed.).

Bejan, A., 2013. *Convection Heat Transfer*, 4th ed.. New Jersey: Wiley.

Corgozinho, I. M., 2015. *Modelagem e simulação computacional de um coletor solar de placa plana utilizando o método dos volumes finitos*. Centro Federal de Educação Tecnológica de Minas Gerais.

Duffie, J., & Beckman, W., 2001. *Solar engineering of thermal processes, 1991*. *Intersciences Publication, USA*, 4th ed.. Hoboken: John Wiley & Sons, Inc.

Gunjo, D. G., Mahanta, P., & Robi, P. S., 2017. CFD and experimental investigation of flat plate solar water heating system under steady state condition. *Renewable Energy*, *106*, 24–36. Elsevier Ltd. Retrieved from http://dx.doi.org/10.1016/j.renene.2016.12.041

INMETRO., 2012. Portaria 301.

International Energy Agency., 2016. *Solar Heat Worlwide*. Gleisdorf. Retrieved from https://www.iea-shc.org/data/sites/1/publications/Solar-Heat-Worldwide-2016.pdf

Launder, B. E., & Spalding, D. B., 1972. *Lectures in mathematical models of turbulence*. (Academic Press, Ed.). London, New York.

Martinopoulos, G., Missirlis, D., Tsilingiridis, G., Yakinthos, K., & Kyriakis, N., 2010. CFD modeling of a polymer solar collector. *Renewable Energy*, *35*(7), 1499–1508. Elsevier Ltd. Retrieved from http://dx.doi.org/10.1016/j.renene.2010.01.004

Missirlis, D., Martinopoulos, G., Tsilingiridis, G., Yakinthos, K., & Kyriakis, N., 2014. Investigation of the heat transfer behaviour of a polymer solar collector for different manifold configurations. *Renewable Energy*, *68*(April 2013), 715–723. Elsevier Ltd. Retrieved from http://dx.doi.org/10.1016/j.renene.2014.03.008

Pandey, K. M., & Chaurasiya, R., 2017. A review on analysis and development of solar flat plate collector. *Renewable and Sustainable Energy Reviews*, *67*, 641–650. Elsevier. Retrieved from

http://dx.doi.org/10.1016/j.rser.2016.09.078

Rangababu, J. A., Kiran Kumar, K., & Srinivasa Rao, S., 2015. Numerical Analysis and Validation of Heat Transfer Mechanism of Flat Plate Collectors. *Procedia Engineering*, *127*, 63–70.

Reynolds, W. C., 1987. *Fundamentals of turbulence for turbulence modeling and simulation. Lecture Notes for Von Karman Institute*.

Shih, T.-H., Liou, W. W., Shabbir, A., Yang, Z., & Zhu, J., 1995. A new k-ϵ eddy viscosity model for high reynolds number turbulent flows. *Computers & Fluids*, *24*(3), 227–238. Pergamon. Retrieved July 18, 2019, from https://www.sciencedirect.com/science/article/pii/004579309400032T

Streicher, W., 2016. Solar thermal technologies for domestic hot water preparation and space heating. *Renewable Heating and Cooling* (pp. 9–39). Elsevier.

Tagliafico, L. A., Scarpa, F., & De Rosa, M., 2014. Dynamic thermal models and CFD analysis for flat-plate thermal solar collectors - A review. *Renewable and Sustainable Energy Reviews*, *30*, 526–537.

United Nations., 2015. Adoption of the Paris Agreement. *Coference of the Paris*. Paris: United Nations.

Versteeg, H. K., & Malalasekera, W., 1995. *An introduction to Computational Fluid Dynamics - The Finite Volume Method*. Longman Scienctific & Technical.

8. RESPONSIBILITY NOTICE

The authors are the only responsible for the printed material included in this paper.